Membranes with a dual structure constituted of titania, zirconia, and both as thin-film selective layers coating the polyacrylonitrile platform

Chabi N. Worou and Zhonglin Chen

ABSTRACT

Three novel thin-film composite (TFC) nanofiltration membranes are prepared using an ultrafiltration membrane (UFM) of organic polymer resin polyacrylonitrile followed by a mineralization process. The UFM was hydrolyzed (H-UFM) and then transferred in dopamine (DA) and tris buffer (TRIS) solutions. DA–TRIS coating is further favorable for the growth of nanoparticles (NPs), titania (TiO_2), and zirconia (ZrO_2) on membrane piece surface. A scanning electron microscope (SEM) was combined with an energy-dispersive spectrometer (EDS) in order to provide important insights into the arrangement and potential functions of NPs, due to their unambiguous chemical signal, for possible characterization and modification of materials at the atomic scale. Depending on whether the top layer is made of TiO_2, ZrO_2, or both, the membranes are called, respectively, TFC-NFTitan, TFC-NFZircon, and TFC-NFTitanZircon. The three membranes under the optimized preparation conditions (30 °C, 12 h of hydrolysis time, 45mmol/L and operating pressure of 0.6 MPa) exhibited high rejection and permeation performance. TFC-NFTitanZircon showed the highest rejection (89–95%) for divalent cations with the salt rejection sequence of $CaCl_2 > MgSO_4 > MgCl_2 > NaCl > Na_2SO_4$, while the permeate flux is not less than $55 L \cdot m^{-2} \cdot h^{-1}$. All three membranes demonstrated long-term durability under 120-h testing.

Key words | EDS, membrane, nanoparticles, salt rejection, SEM, thin-film composite

Chabi N. Worou (corresponding author)
Zhonglin Chen
State Key Laboratory of Urban Water Resource and Environment, School of Environment,
Harbin Institute of Technology,
Harbin 150090,
China
E-mail: *worouccc@yahoo.fr*; *worouccc@stu.hit.edu.cn*

HIGHLIGHTS

- Thin-film composite nanofiltration membrane (NFM) for salt rejection.
- Novel *in situ* NFM fabrication using the insights provided by a scanning electron microscope combined with an energy-dispersive spectrometer on the arrangement and potential functions of nanoparticles.
- Modification of an ultrafiltration membrane to the NFM for salt removal.
- Organic–inorganic NF preparation using a mineralization process.

doi: 10.2166/aqua.2021.147

GRAPHICAL ABSTRACT

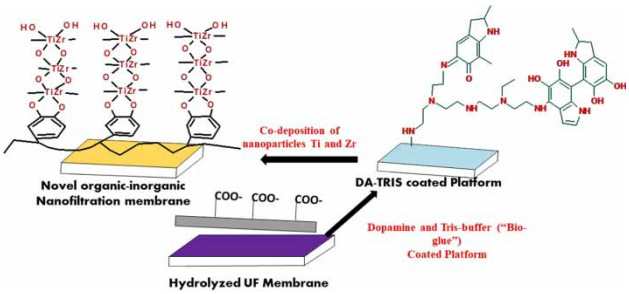

INTRODUCTION

Nanofiltration (NF) is a pressure-driven process with properties lying between those of ultrafiltration (UF) and reverse osmosis (RO) (Nazia *et al.* 2020). The NF process was first explored during the late 1980s (Siddique *et al.* 2020; Yang *et al.* 2020b). Many things have changed over time; for example, the transmembrane pressure for NF membranes (NFMs) was initially in the range of 5–20 bar (Amirilargani *et al.* 2016) and nowadays can reach 40 bar (Marchetti *et al.* 2014). A variety of advantages such as low transmembrane pressure, high permeation flux, and high retention rate toward multivalent salts, and low investment (in comparison with the RO process) made NF to be used in various areas (Li *et al.* 2011; Luo & Wan 2013; Zinadini *et al.* 2017; Guo *et al.* 2020; Mi *et al.* 2020). Nowadays, different methods are used to prepare or modify NFMs. Among these techniques, interfacial polymerization (Yuan *et al.* 2020), nanoparticle (NP) incorporation (Singh & Mehata 2020), UV treatment (Nigiz & Kibar 2020), and layer-by-layer process (Guo *et al.* 2020) are more and more explored. All the methods used in the NF process aimed at developing membranes with higher selectivity, better rejection tendency, higher permeation flux, and also overcoming sometimes fouling issues. Despite the significant development of the NF process in laboratories and water treatment plants, there are still some issues to be addressed. To improve NFM utilization, Van der Bruggen *et al.* have studied several membrane parameters such as membrane lifetime and chemical resistance, membrane fouling, and membrane rejection (Van der Bruggen *et al.* 2008).

Most of the ideal NFMs are thin-film composite (TFC) membranes with support and a thin-film selective layer (Zhang *et al.* 2014a, 2014b; Lv *et al.* 2016; Zhao *et al.* 2020a, 2020b). Organic–inorganic TFC-NFMs have usually been synthesized by dispersing inorganic fillers in the polymer selective layer through blending, the sol–gel method, or *in situ* formation (Spijksma *et al.* 2006; Zheng *et al.* 2011; Vinh-Thang & Kaliaguine 2013; Fukumoto *et al.* 2014; Siddique *et al.* 2014; Jeon & Lee 2020; Karami *et al.* 2020). To successfully manufacture this type of membrane, a judicious choice of the organic support, of the inorganic NPs, and of what would play the role of 'bio-glue' for good adhesion between the substrate and the inorganic top layer is essential. In this study, as an organic substrate, a UF membrane polyacrylonitrile (PAN) has been used; and for inorganic NPs, both dioxide of titanium (TiO_2) and dioxide of zirconium (ZrO_2) have been chosen.

NPs have received much attention recently due to their unique properties in terms of catalytic activity, photoemission, and antimicrobial. NP-incorporated membranes have gained attention due to their ability to increase membrane permeability, mechanical properties, hydrophilicity, and selectivity in some cases. The NPs, which are commonly reported in NFMs fabrication, are ZrO_2, TiO_2, silica (SiO_2), silver, and zinc oxide (ZnO) (Mohammad *et al.* 2015; Worou *et al.* 2021a, 2021b). In the case of TiO_2, NF composite membranes have been prepared recently with a polyethyleneimine (PEI)-NP hybrid active layer through mineralization. Inorganic

precursors tetra-*n*-butyl titanate and tetraethoxysilane were applied, respectively, to prepare PEI-TiO_2 and PEI-SiO_2 composite membranes (Zhang *et al.* 2014c). On the other hand, optimized TiO_2 NFMs showed a pure water permeability as high as 48 $L \cdot m^{-2} \cdot h^{-1} \cdot bar^{-1}$. Molecular layer deposition (MLD) was used as a novel and highly controllable method to prepare TiO_2 NFMs with approximately 1 nm pores for water purification. According to Song *et al.*, MLD, as a new TiO_2 NFM preparation technique, exhibits great potential to realize excellent control of membrane composition, thickness, and potentially pore sizes in a scalable way (Spijksma *et al.* 2006; Xia *et al.* 2007; Song *et al.* 2016). The ZrO_2 was also adopted as an inorganic selective layer in this experiment because it is widely used for its proven high-performance filtration membranes as an inorganic component with superior chemical, physical, and thermal stability, and good hydrophilicity (Ou *et al.* 2011; Mi *et al.* 2014). The presence of both (TiO_2 and ZrO_2) NPs favored an enhancement of the thermal and structural stabilities. As a result of the hybridization and cross-linkage, the membrane performances such as permeation flux and retention rate were improved, as also long-term operating stability. Mohammad *et al.* demonstrated that hybrid nanomaterials were much better than the normal application of NPs (Mohammad *et al.* 2015).

The UF membrane of PAN, also known as polyvinyl cyanide or Creslan 61, was hydrolyzed in a sodium hydroxide (NaOH) solution and then immersed into a hydrochloric acid solution to prepare its surface to receive a bio-glue with great adhesive strength. In this case, dopamine (DA) hydrochloride, a well-known bio-glue, can be oxidized in an alkaline environment, and it forms a polymer-like coating on various substrates with great adhesive strength. Lv *et al.* used in their work PEI as a crosslinking component to promote the homogeneous polymerization of DA and uniform co-deposition of PDA-PEI (Lv *et al.* 2016). To avoid this self-aggregation of DA and to obtain a smooth and dense selective layer, DA hydrochloride was dissolved in Tris–HCl buffer solution. Thus, three different TFC membranes, TFC-NFTitan, TFC-NFZircon, and TFC-NFTitanZircon, have been prepared, respectively, with TiO_2, zirconia (ZrO_2), and both (TiO_2, ZrO_2) as the inorganic selective top layer.

EXPERIMENTAL

Materials and agents

The UF membrane of PAN, also known as polyvinyl cyanide or Creslan 61 flat-sheet ($L =$ 101.6 cm; $l =$ 96 cm), with a-molecular weight cut-off of 100 kDa, and a pore size of 0.076 μm, is a commercial product of Jiangsu Kaimi Membrane Technology Co. Ltd (China) or is available in Shanghai Mega Vision Membrane Engineering & Technology Co. Ltd (China). DA hydrochloride and Tris buffer solution were purchased from Aladdin (China). Titanium sulfate hydrate ($Ti{\cdot}SO_4{\cdot}H_2O$), hydrochloric acid solution (12 mol/L), zirconium sulfate tetrahydrate ($Zr(SO_4)_2{\cdot}4H_2O$), ethanol, and NaOH were all obtained from Sino Pharm Chemical Reagent Co., Ltd and used as received.$MgCl_2$, $CaCl_2$, $MgSO_4$, Na_2SO_4, and NaCl were supplied by Aladdin (China).

Steps of TFC-NFTitan, TFC-NFZircon, and TFC-NFTitanZircon preparation

Fabrication of hydrolyzed PAN UF membrane and DA/TRIS-coated hydrolyzed PAN UF membrane

The PAN UF membrane (UFM) has been hydrolyzed in NaOH solution (1.5 mol/L) for 1 h 30 min at 50 °C and then immersed into hydrochloric acid solution (2 mol/L) for another 1 h 30 at 30 °C. The resulted membrane is called H-UFM, hydrolyzed PAN UFM, as shown in Figure 1.

DA hydrochloride was dissolved in Tris–HCl buffer solution (pH = 8.4; 55 mmol/L) to prepare another solution used later for deposition with a total concentration of 1.9 g/L, and the deposition time was set at 2 h. These conditions are based on the mass of DA HCl–Tris buffer solution deposited on the membrane surface and the thickness of the coating layer. The circular pieces of UFM with a diameter of 61 mm were pre-wetted by ethanol for 30 min and then transferred into the freshly prepared DA HCl–Tris buffer solution (DA–TRIS) and shaken at 30 °C for 2 h. The synthesized platforms (DA–TRIS-coated H-UFMs) were washed by deionized (DI) water and dried in an ambient environment (Figure 1).

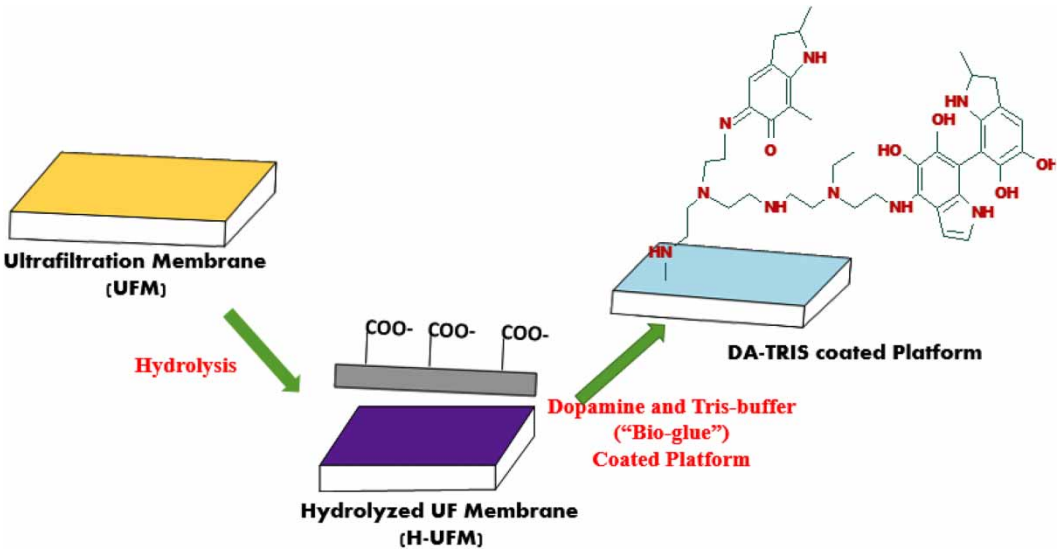

Figure 1 | Membrane platform preparation (in steps 1 and 2 before the growth of nanoparticles).

Organic–inorganic TFC-NFTitan, TFC-NFZircon, and TFC-NFTitanZircon synthesis

Finally, solutions of $Ti{\cdot}SO_4{\cdot}H_2O$ and $Zr\ (SO_4)_2{\cdot}4H_2O$ were prepared.

- *Solution 1*: $Ti{\cdot}SO_4{\cdot}H_2O$ was dissolved in a hydrochloric solution (45 mmol/L) with a concentration of 5 mmol/L.
- *Solution 2*: $Zr\ (SO_4)_2{\cdot}4H_2O$ was dissolved in a hydrochloric solution (45 mmol/L) with a concentration of 5 mmol/L.
- *Solution 3*: Both solutions 1 and 2 were used separately for deposition.

Subsequently, some pieces of DA–TRIS-coated platform membranes were immersed in *solution 1* at room temperature (30 °C) for 12 h. These membranes were rinsed several times and dried in a vacuum oven overnight. The resulted membrane, in this case, is called *TFC-NFTitan*. The preparation process is schematically presented in Figure 2.

Other pieces of DA–TRIS-coated PAN membranes were immersed in solution 2 at room temperature (30 °C) for 12 h. These membranes were also rinsed several times and dried in a vacuum oven overnight. The resulted membrane is called *TFC-NFZircon*. The preparation process is schematically presented in Figure 2.

The final pieces of DA–TRIS-coated HPES membranes were immersed into solution 1 at room temperature (30 °C) for 6 h and then transferred into solution 2 under the same conditions (temperature, $T = 30\ ^\circ C$; hour, $t = 6$ h). The resulted membrane is called *TFC-NFTitanZircon*, and the preparation process is schematically presented in Figure 2.

Membrane characterization

Field emission scanning electron microscopy

Field emission scanning electron microscopy (FESEM) was used for DA–TRIS-coated platform, TFC-NFTitan, TFC-NFZircon, and TFC-NFTitanZircon membranes' surface morphology investigation, and the results were written down and interpreted (Figure 4).

Energy-dispersive spectrometer

The elements observed on the membrane's surface were carbon (C), oxygen (O), nitrogen (N), titanium (Ti), and zirconium (Zr). Each element of an energy-dispersive spectrometer (EDS) has its X-ray characteristic wavelength. The size of the characteristic wavelength depends on the characteristic energy ΔE released during the energy-level transition. The energy spectrometer uses X rays of different

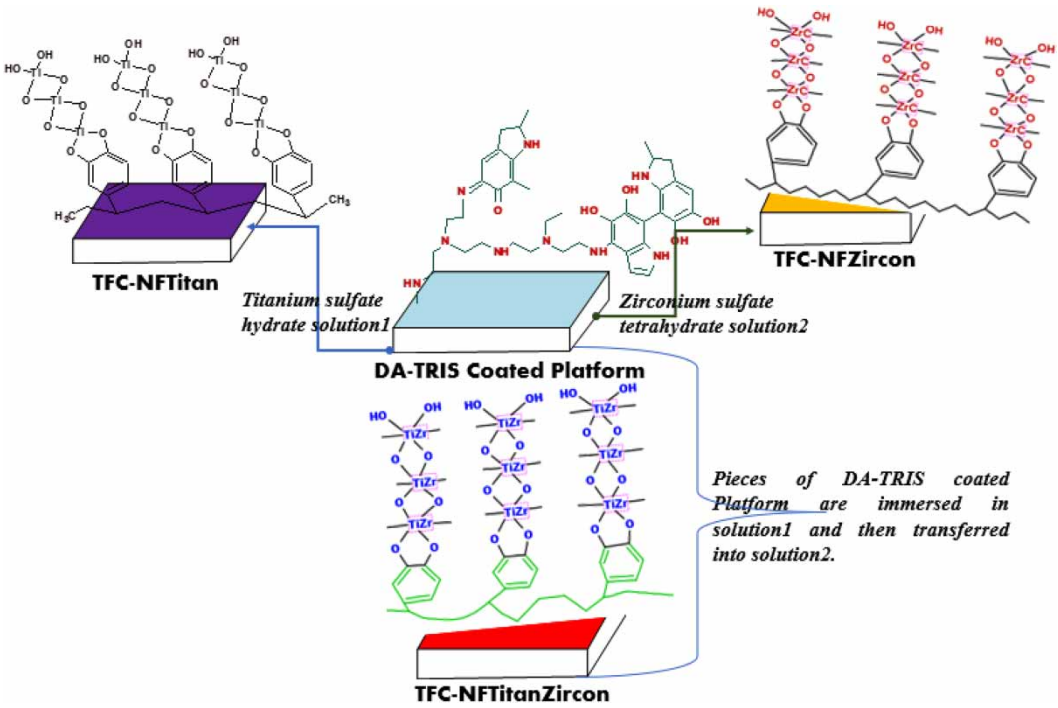

Figure 2 | Final step of TFC-NFTitan, TFC-NFZircon, and TFC-NFTitanZircon membrane preparation.

elements. The characteristics of photon characteristic energy are different for component analysis.

Atomic force microscopy

An atomic force microscopy (AFM, MultiMode Vecco, USA) is used to observe the morphology and roughness of the membranes in a tapping mode using silicon tips with nanometer-scale resolution in air. Four membranes' roughness has been measured and reported in this work, DA–TRIS-coated Platform, TFC-NFTitan, TFC-NFZircon, and TFC-TitanZircon.

Water contact angle

Dynamic water contact angle (WCA) measurements were performed with an EasyDrop Instrument (DropMeter A-200 contact angle system; MAIST Vision Inspection & Measurement Co. Ltd, China) at room temperature using the drop method, in which a drop of water was deposited on the surface of a piece of the membrane using a micropipette. The contact angles were measured automatically by a video camera in the instrument using drop shape analysis software. Several measurements on each membrane piece were performed. Five membrane pieces were immersed in ethanol for 30 min and dried in an oven before measuring their contact angle (Figure 5(a)).

Zeta potential

The electrokinetic analyzer (SurPASS Anton Paar, GmbH, Austria) has been used to detect the charging property of the membranes' surface. Five samples have had their zeta potential measured: H-UFMs, DA–TRIS-coated platform, TFC-NFTitan, TFC-NFZircon, and TFC-NFTitanZircon, as made clear in Figure 5(b).

Stability test in various solvents

Immersion tests were carried out with each membrane to determine their long-stability in solvents for a 120 h test at room temperature. Every 12 h, both water flux and rejection were measured for each novel organic–inorganic TFC-NF membrane. The membranes withdrawn after this period were carefully rinsed with water and dried at atmospheric conditions.

Membrane performance evaluation

The membrane performance of TFC-NFTitan, TFC-NFZircon, and TFC-NFTitanZircon was evaluated by using a laboratory-scale cross-flow flat membrane module under 0.6 MPa at 30 ± 1 °C. The effective area was 29.22 cm^2 for each sample. Various salts, including $MgCl_2$, $CaCl_2$, $MgSO_4$, Na_2SO_4, and NaCl, were dissolved in DI water at a concentration of 1,500 mg/L and used as feed solutions with a fixed cross-flow rate of 30 L/h. The water flux (F_w, $L \cdot m^{-2} \cdot h^{-1}$) and rejection ($R$, %) were calculated by the following equations:

$$F_w = \frac{Q}{A \cdot t} \quad (1)$$

where Q, A, ΔP, and t represent the volume of permeated water, the effective membrane area, the transmembrane pressure, and the permeation time, respectively.

$$R = \left(1 - \frac{C_p}{C_f}\right) \times 100\% \quad (2)$$

where C_p and C_f are, respectively, the solute concentrations in permeate and feed sides that were measured by using a conductivity meter (Metrohm AG) and an inductively coupled plasma optical emission spectrometer (Optima 7300 DV, PerkinElmer, USA). All results presented were repeated at least three times. The pieces of organic–inorganic TFC-NFTitan, TFC-NFZircon, and TFC-NFTitanZircon membranes were tested on the cross-flow flat membrane module for 120 h continuously by measuring the water flux and salt rejection every 12 h.

RESULTS AND DISCUSSION

TFC-NFTitan, TFC-NFZircon, and TFC-NFTitanZircon membrane characterization

To provide important insights into the arrangement and potential functions of NP layer-coated substrates, a scanning electron microscope (SEM) has been combined with an EDS. In Figure 3, the results of energy spectrum analysis for the TFC-NFTitanZircon membrane are reported. The

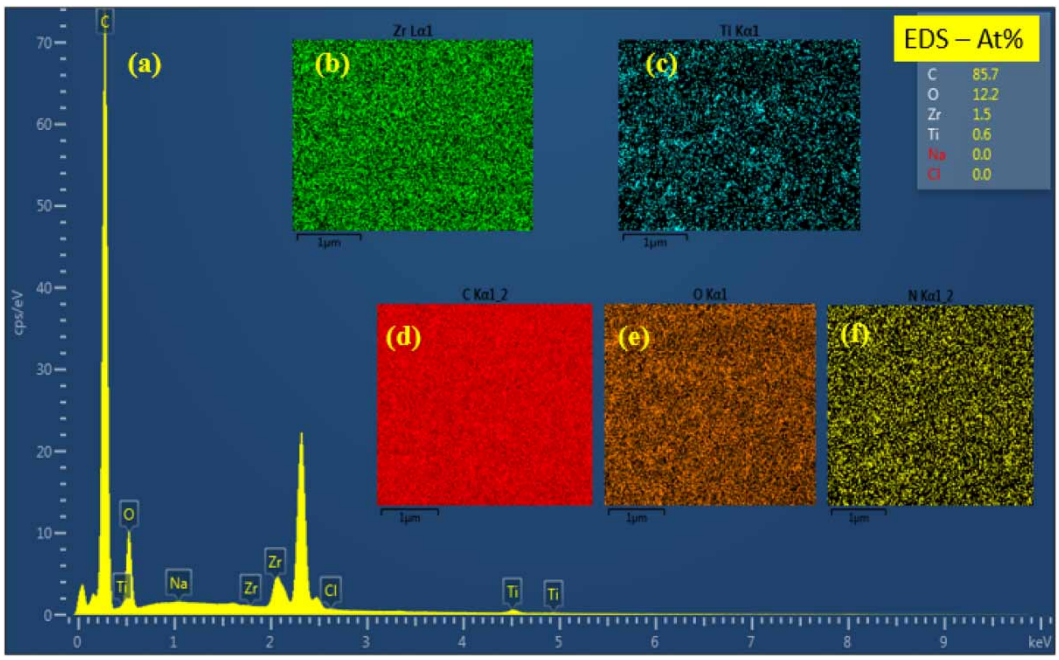

Figure 3 | (a) Energy spectrum analysis results of the TFC-NFTitanZircon and the sample table surface elements containing (b) Zr, (c) Ti, (d) C, (e) O, and (f) N.

EDS identified five elements such as C, O, N, Ti, and Zr due to its unique X-ray signals. It is, therefore, possible to characterize and modify the materials at the atomic scale, providing unparalleled insight into the behavior of nanomaterials and particles (Supplementary Material, Figures S1 and S2). In Figure 3, the individual atomic positions can be distinguished by their unambiguous chemical signal. The individual atomic columns are not only visible but also distinct from their neighbors due to their high contrast. In Supplementary Material, Figures S1 and S2, the results of energy spectrum analysis for TFC-NFTitan and TFC-NFZircon, respectively, are reported.

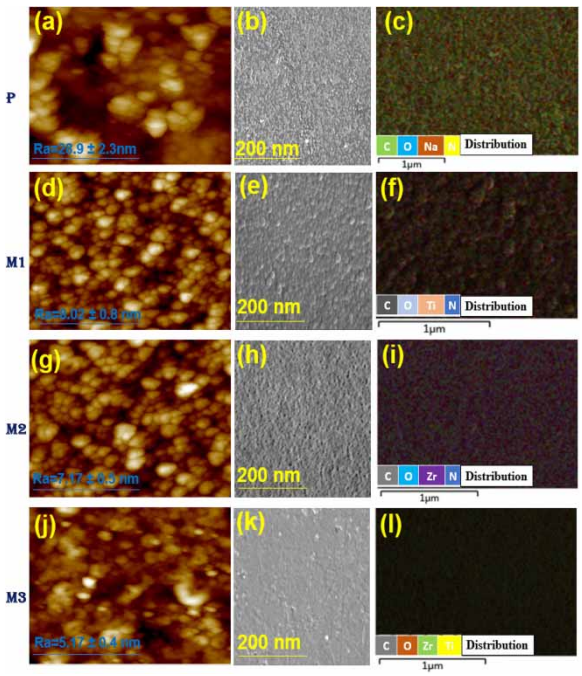

Figure 4 | AFM images (a, d, g, j), FESEM (b, e, h, k), and element distribution (c, f, i, l), respectively, of DA–TRIS-coated platform (P), TFC-NFTitan (M1), TFC-NFZircon (M2), and TFC-NFTitanZircon (M3) membranes.

Figure 4 shows surface roughness, morphology, and elements repartition for DA–TRIS-coated Platform (P), TFC-Titan (M1), TFC-Zircon (M2), and TFC-TitanZircon (M3). These characteristics are of great importance in NF. Membrane (P) is the roughest ($R_a = 28.9$ nm) according to the AFM image (Figure 4(a)), which the SEM (Figure 4(b)) seems to confirm. The membrane surface has changed significantly with the formation of the TiO_2 top layer in Figure 4(d) and 4(e). The roughness decreased significantly from 28.9 to 8.02 nm (Figure 4(f)). The remarkable difference between membrane P and membranes M1, M2, and M3 is due to the fact that P is a UF substrate, while the others are NF membranes. A dense and smooth selective layer like in the case of TFC-NFTitanZircon (M3) is beneficial for outstanding TFC-NFMs in general. It was demonstrated further in the forthcoming paragraph that M3 provides the highest rejection performance in comparison with M1 and M2.

The WCA was used to evaluate the wettability of the H-UFM, DA–TRIS-coated platform (P), TFC-NFTitan (M1), TFC-NFZircon (M2), and TFC-NFTitanZircon (M3) (Figure 5(a)). The H-UFM shows the best hydrophilicity

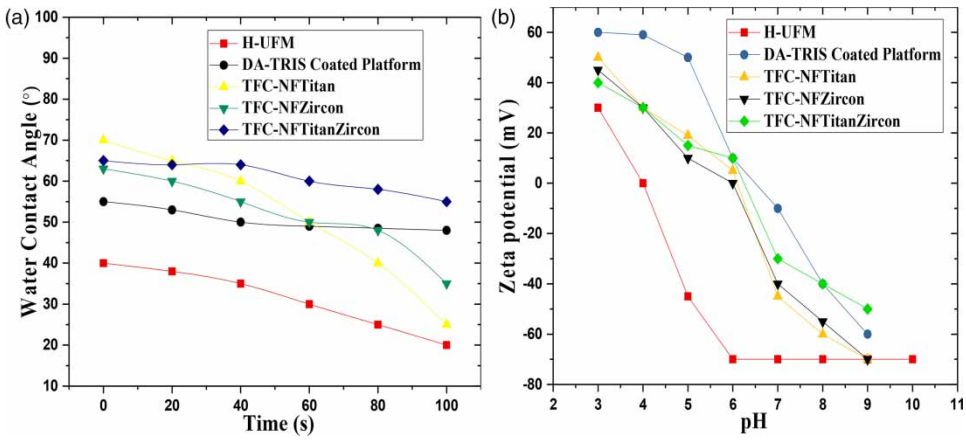

Figure 5 | WCA (a) and zeta potential at various pH (b) of H-UFM, DA–TRIS-coated platform, TFC-NFTitan, TFC-NFZiron, and TFC-NFTitanZircon.

due to its hydrophilic groups combining with the porous structure which are covered later by DA–TRIS coating. As the top layer becomes more and more smooth and dense, an increase in WCA results. This phenomenon is further enhanced after the NPs' TiO_2 and ZrO_2 layers were fabricated on the mussel-inspired platform surface, which is ascribed to the more dense and smooth structures for the three novel fabricated membranes. Although the novel TFC NFM is the least hydrophilic of all the membranes investigated, it still exhibits good hydrophilicity (WCA < 66) and can, therefore, be fast spread out by water, which is good for their permeation performance (Somvanshi *et al.* 2020). On the other hand, Donnan's potential at the interphase of solution and membrane excludes co-ions from the NFM (Sanchez *et al.* 2005; Luo & Wan 2013). Thus, the surface charge plays a crucial role in organic–inorganic TFC NFM preparation.

Figure 5(b) demonstrates the zeta potentials of the studied membranes at various pH values. At all pH values, the H-UFM exhibits the lowest zeta potential in comparison with the other membranes. The electronegativity (−70 mV) of H-UFM when pH is between 6 and 8.5 is favorable for the co-deposition of DA–TRIS. As observed in Figure 5(b), zeta potential decreases dramatically for the DA–TRIS-coated platform, which is mainly due to the introduction of abundant amino groups from the tris buffer. The potential reduces slightly for TFC-NFTitan, TFC-NFZircon, and TFC-NFTitanZircon after introducing the NP layers on the platform surface, as the electro-positivity of the TiO_2 and ZrO_2 NPs is slightly more than that of the DA–TRIS coating (Lv *et al.* 2016). These results demonstrate that the novel prepared organic–inorganic TFC-NFMs are positively charged during the NF process conducted at pH 6.0.

Permeability of TFC-NFTitan, TFC-NFZircon, and TFC-NFTitanZircon membranes

The three different TFC membranes, TFC-NFTitan, TFC-NFZircon, and TFC-NFTitanZircon, have been prepared, respectively, with TiO_2, ZrO_2, and both (TiO_2 and ZrO_2) as the inorganic selective top layer by the controlled hydrolysis process of $Ti{\cdot}SO_4{\cdot}H_2O$ and $Zr\ (SO_4)_2{\cdot}4H_2O$. The equilibrium reactions that occur are as follows:

For TiO_2:

$$[TiO(SO_4)] + 3H_2O \rightarrow 2H^+ + [Ti(OH)_4SO_4]^{2-} \quad (3)$$

$$[Ti(OH)_4SO_4]^{2-} \rightarrow TiO_2 + SO_4^{2-} + 2H_2O \quad (4)$$

For ZrO_2:

$$2[Zr(SO_4)_2] + 3H_2O \rightarrow [Zr_2(OH)_3(SO_4)_4]^{3-} + 3H^+ \quad (5)$$

$$[Zr_2(OH)_3(SO_4)_4]^{3-} + 3OH^- \rightarrow Zr_2(OH)_6SO_4 + 3SO_4^{2-} \quad (6)$$

$$Zr_2(OH)_6SO_4 + 2OH^- \rightarrow 2ZrO_2 + SO_4^{2-}\ 4H_2O \quad (7)$$

NFMs are usually applied to separate ions with different valences from water and the retention performance of salts can also reflect the charge characteristics of membranes (Farooq *et al.* 2020; Tofighy & Mohammadi 2020; Yang *et al.* 2020b; Zhao *et al.* 2021). Thus, in this section, various salt solutions (1, 500 mg/L) were used to evaluate the rejection performance of the three novel organic–inorganic TFC-NFMs. The water flux and salt rejection of TFC-NFTitan, TFC-NFZircon, and TFC-NFTitanZircon membranes with $MgCl_2$, $CaCl_2$, $MgSO_4$, Na_2SO_4, and NaCl are shown in Figure 6. The rejection ratio reaches as high as 94% for bivalent cations, although it is lower than 30% for monovalent cations. The order of salt rejection of TFC-NFTitan is $MgCl_2 > MgSO_4 > CaCl_2 > NaCl > Na_2SO_4$, as exhibited in Figure 6(a), whereas those of TFC-NFZircon and TFC-NFTitanZircon are, respectively, $MgCl_2 > CaCl_2 > MgSO_4 > NaCl > Na_2SO_4$ and $CaCl_2 > MgSO_4 > MgCl_2 > NaCl > Na_2SO_4$ in Figure 6(b) and 6(c). These results are reasonable in those NF processes mainly determined by Donnan and dielectric effects (Wang *et al.* 2012). TFC-NFTitanZircon exhibits the highest rejection toward both divalent cations (between 89 and 95%) and monovalent cations. The novel organic–inorganic TFC-NFMs are positively charged at pH 6.0 and hence possess a better rejection of multivalent cations than anions (Figure 5(b)). The water flux value for each salt is quite similar under the three novel membranes and is set at 50, 60, and 58 $L \cdot m^{-2} \cdot h^{-1}$, respectively, for TFC-NFTitan, TFC-NFZircon, and TFC-NFTitanZircon. Figure 6(d)

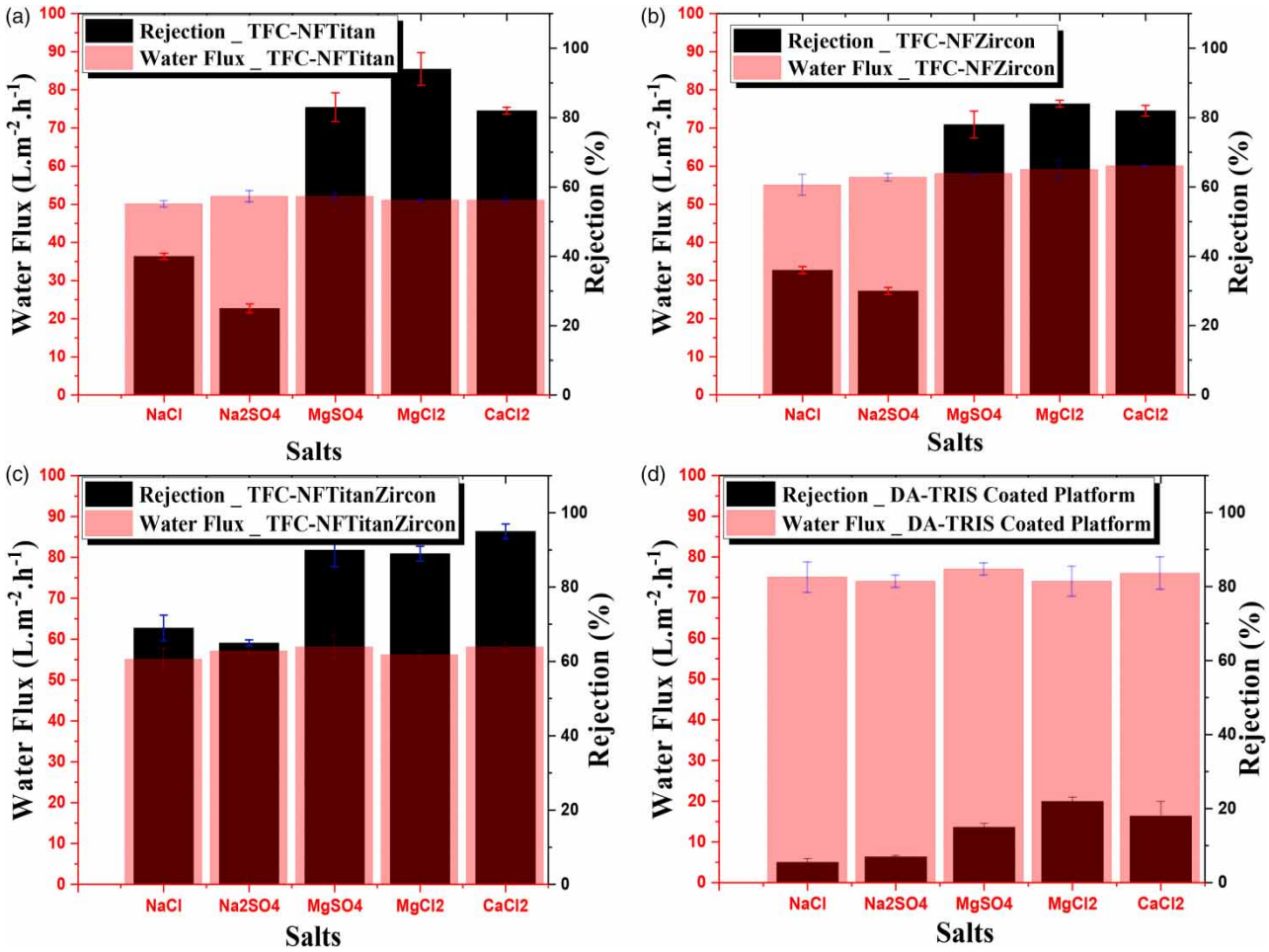

Figure 6 | Different salt rejection performance of (a) TFC-NFTitan, (b) TFC-NFZircon, (c) TFC-NFTitanZircon, and (d) DA–TRIS-coated platform membranes.

depicts the water flux and salt rejection of DA–TRIS-coated platform membrane with an extremely high flux ($>75\ L \cdot m^{-2} \cdot h^{-1}$) but poor salt rejection.

The synthesized NF membranes' (TFC-NFTitan, TFC-NFZircon, and TFC-NFTitanZircon) water flux and rejection performance are reported in Table 1, together with those of some earlier reported ones.

TFC-NFTitanZircon is the best performing of the three membranes synthesized in this study. Thus, it can be deduced that the co-deposition of NPs seems to promote

Table 1 | Water flux and rejection performance of membranes prepared in this work and some earlier reported ones

Membranes	Water flux ($L \cdot m^{-2} \cdot h^{-1}$)	Rejection (%)	References
TFC-NFTitan	51	83	This study
TFC-NFZircon	59	80	This study
TFC-NFTitanZircon	56	96	This study
PAN-ZrO_2	60	>90	Lv *et al.* (2016)
	4.2	81.9	Vatanpour *et al.* (2012)
PAN-functionalized MWCNTs	24	80	Vatanpour *et al.* (2014)

the performance of NF membranes. Also, this point of view is widely shared by Polyakov *et al.* in their recent work on direct co-deposition of nano-sized NPs (Polyakov *et al.* 2020) and Cui *et al.* on Mussel-Inspired co-deposition of DA/SiO_2 NPs (Cui *et al.* 2020).

Generally, synthesized NF membranes are either efficient at rejecting ions or display high flux permeate release (Table 1); if the scientific world studies NPs, their affinity, and the stoichiometric conditions of their co-deposition, it could be very beneficial for the development of a next high-performance generation of NF membranes.

Effects of operating conditions on the permeability of TFC-NFTitan, TFC-NFZircon, and TFC-NFTitanZircon

Thermal stability of novel organic–inorganic TFC-NFMs

The effect of operating temperature on these membranes is shown in Figure 7(a), under the operating pressure of 0.6 MPa. It was observed that the water flux of all novel organic–inorganic TFC-NFMs increased quickly about two times between 10 and 30 °C and just about one time between 30 and 60 °C. Since it is not very comfortable to carry out

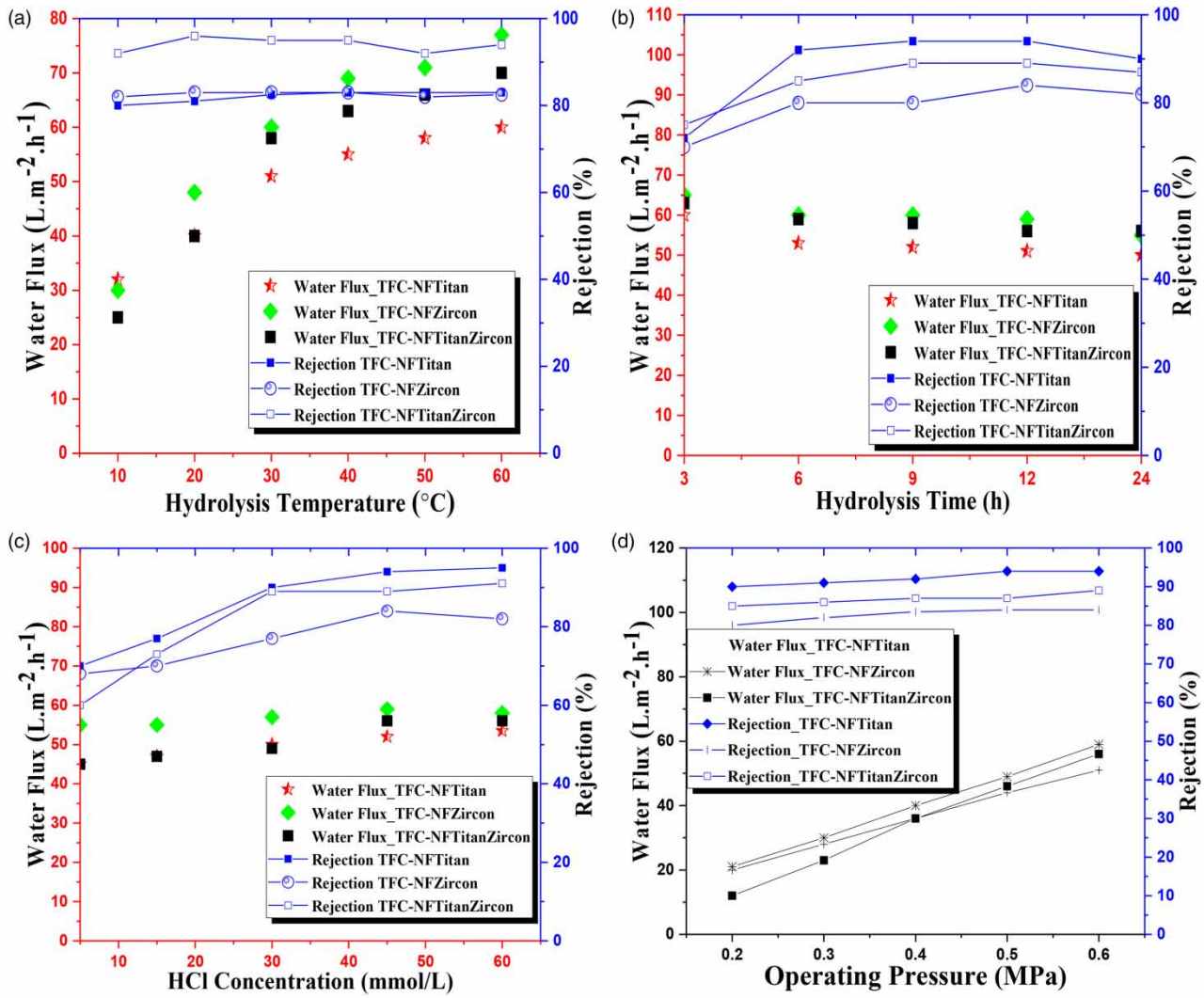

Figure 7 | Effects of operating conditions on the permeability of TFC-NFTitan, TFC-NFZircon, and TFC-NFTitanZircon: (a) hydrolysis temperature, (b) hydrolysis time, (c) HCl concentration, and (d) operating pressure. Test conditions: [$MgCl_2$] = 1,500 mg/L; 0.6 MPa; cross-flow rate = 30 L/h; pH = 6.0.

these operations at very high temperatures when it comes to large-scale production, the operating temperature has been set at 30 °C. This increase in water flux was mainly due to the diffusion coefficients, which increased, while the viscosity coefficients of water solution decreased with the increase in temperature (Athar *et al.* 2020; Kondoh *et al.* 2020; Nazir *et al.* 2020; Pavon *et al.* 2020). The quite constant rejection of the TFC-NFTitan, TFC-NFZircon, and TFC-NFTitanZircon membranes, even when the operating temperature reached 60 °C, partly demonstrated the good thermal stability of the novel organic–inorganic TFC-NFMs. Therefore, it is possible to enhance the water flux by increasing the operating pressure (Figure 7(d)) and temperature with constant salt rejection.

Hydrolyze time effect on novel organic–inorganic TFC-NFMs

The efficacity of the novel organic–inorganic TFC-NFMs was evaluated with a cross-flow NF process. The NP layers are formed by controlling the hydrolysis of $Ti{\cdot}SO_4{\cdot}H_2O$ and $Zr(SO_4)_2{\cdot}4H_2O$ according to Equations (1)–(5). Therefore, the performance of TFC-NFTitan, TFC-NFZircon, and TFC-NFTitanZircon will be influenced by the hydrolysis parameters such as hydrolysis time and acid chloride concentration. In Figure 7(b), both a dramatic decrease in water flux and a dramatic increase of salt[$MgCl_2$] rejection were noticed at the beginning of the experiment (the first 3 h). This state of affairs is understandable and is due to the change in the nature of the membranes from a UF membrane to a NF membrane. For membranes TFC-NFTitan and TFC-NFTitanZircon, the salt rejection peak was reached around 9 h but changed not till 12 h, whereas it was necessary to wait until 12 h before reaching the rejection peak with the TFC-NFTitanZircon membrane. However, both the water flux and the rejection changed little as the hydrolysis time extended to 24 h. Therefore, 12 h was chosen as the optimal hydrolysis time considering both the water flux and rejection performance of the three novel organic–inorganic TFC-NFMs.

Effect of HCl concentration on novel organic–inorganic TFC-NFMs

Figure 7(c) exhibits the effect of HCl concentration on novel fabricated NFMs. According to Equations (1)–(5) relative to the hydrolysis mechanism of Ti^{2+} and Zr^{2+} in water, it was indicated that low pH will reduce the reaction rate in the titanium sulfate and zirconium sulfate solutions, respectively, and resulted in TiO_2 and ZrO_2 NPs on the DA–TRIS-coated membranes surface. For TFC-NFTitan and TFC-NFZircon, both water flux and rejection increase with HCl concentration in the range of 0–45 mmol/L. But, from 45 to 60 mmol/L, the rejection increased slightly and decreased in the same order for each of them, respectively. For membrane TFC-NFTitanZircon, the water flux increased with HCl concentration; the rejection increased, while the HCl concentration increased from 0 to 30 mmol/L and remained constant between 30 and 60 mmol/L. Thus, it is very easy to find the optimal concentration of HCl for the three membranes. A concentration of 45 mmol/L satisfied the performance of these membranes toward both rejection and high-water flux.

Operating pressure

Figure 7(d) shows the effect of operating pressure on water flux and rejection of the novel prepared NFMs while the operating temperature was set at 30 °C. It was observed that the water flux of the TFC-NFTitan, TFC-NFZircon, and TFC-NFTitanZircon membranes nearly increased linearly, respectively, from 20 to 51 $L{\cdot}m^{-2}{\cdot}h^{-1}$, 21 to 59 $L{\cdot}m^{-2}{\cdot}h^{-1}$, and 12 to 56 $L{\cdot}m^{-2}{\cdot}h^{-1}$ as the operating pressure increased from 0.2 to 0.6 MPa. Thus, the water flux increased with the operating pressure as predicted by the Spiegler–Kedem Model (Spiegler & Kedem 1966). On the other hand, the rejection rates increased very slightly by 13, 10.5, and 9.1%, respectively, for membranes TFC-NFTitan, TFC-NFZircon, and TFC-NFTitanZircon.

Long-term stability test on novel organic–inorganic TFC-NFMs fabricated

To evaluate the long-term stability of the TFC-NFTitan, TFC-NFZircon, and TFC-NFTitanZircon membranes, a continuous filtration test of 120 h was carried out on each membrane. The results are presented in Figure 8. For test conditions, the salt solutions used are, respectively, [$MgCl_2$], [$CaCl_2$], and [NaCl], since TFC-NFTitan, TFC-NFZircon, and TFC-NFTitanZircon exhibited the best

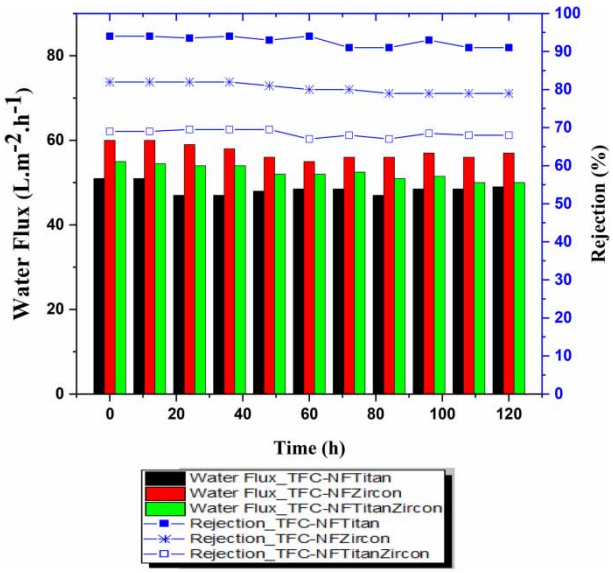

Figure 8 | Long-term stability test on novel fabricated membranes. Test conditions: 0.6 MPa; cross-flow rate = 30 L/h; pH = 6.0. [$MgCl_2$] = 1,500 mg/L for TFC-NFTitan; [$CaCl_2$] = 1,500 mg/L for TFC-NFZircon; and [NaCl] = 1,500 mg/L for TFC-NFTitanZircon.

performance rejection toward the latter ones (concentration [1,500 mg/L], 30 °C, pH = 6.0, 0.6 MPa, and cross-flow rate = 30 L/h). Globally, for all the three membranes, both the water flux and the rejection exhibited satisfying long-term stability. The water flux of the TFC-NFTitan membrane (although the lowest) remains quite constant over time for a decrease of less than 2%. The water flux for both TFC-NFZircon and TFC-NFTitanZircon membranes, from the beginning to the end of the long-term operation, varied very slightly and remained high (more than 50 $L{\cdot}m^{-2}{\cdot}h^{-1}$) till the end of the test. During the 120 h test, all three membranes performed very well at the nearly constant rejection rates of 93, 80, and 68%, respectively, for membranes TFC-NFTitan, TFC-NFZircon, and TFC-NFTitanZircon. The good durability of these membranes is closely related to the interfacial compatibility between the NPs (TiO_2 and ZrO_2) as selective layers and the support surface UF membrane through the robust and multiple binding forces between DA–TRIS-coating H-UFM. The high rate of rejection and the low water flow rate of the TFC-NFTitan membrane are certainly due to the greater fineness of the TiO_2 NPs compared with that of the ZrO_2 NPs. Thus, this test made it possible to demonstrate the long-term effectiveness of the novel TFC-NFMs prepared in this work.

CONCLUSION

Three new organic–inorganic TFC-NF membranes were manufactured by the *in situ* formation approach formed with Ti, Zr, and a co-deposition of these two NPs. The three novel membranes under the optimized preparation conditions (30 °C, 12 h of hydrolysis time, 45 mmol/L, and operating pressure of 0.6 MPa) exhibited high rejection and permeation performance. All three membranes demonstrated long-term durability under a 120-h testing. TFC-NFTitanZircon obtained by the co-deposition of both NPs showed the highest rejection (89–95%) for divalent cations with the salt rejection sequence of $CaCl_2 > MgSO_4 > MgCl_2 > NaCl > Na_2SO_4$, while the water flux is not less than $55 L \cdot m^{-2} \cdot h^{-1}$. We strongly recommend that the scientific world begin to study much more in the future on how to combine two or more NPs according to their affinity, leading to more efficient and more robust membranes.

ACKNOWLEDGMENTS

The authors would like to thank our group members for their kind help and suggestions.

CONFLICT OF INTEREST

The authors declare no competing financial interest.

DATA AVAILABILITY STATEMENT

All relevant data are included in the paper or its Supplementary Information.

REFERENCES

Amirilargani, M., Sadrzadeh, M., Sudhölter, E. & De Smet, L. 2016 Surface modification methods of organic solvent nanofiltration membranes. *Chemical Engineering Journal* **289**, 562–582.

Athar, K., Doranehgard, M. H., Eghbali, S. & Dehghanpour, H. 2020 Measuring diffusion coefficients of gaseous propane in heavy oil at elevated temperatures. *Journal of Thermal Analysis and Calorimetry* **139** (4), 2633–2645.

Cui, X., Ma, L. & Wu, G. 2020 Mussel-inspired co-deposition of polydopamine/silica nanoparticles onto carbon fiber for improved interfacial strength and hydrothermal aging resistance of composites. *Polymers* **12** (3), 712.

Farooq, U., Upadhyaya, L., Shakeel, A., Martinez, G. & Semsarilar, M. 2020 pH-responsive nano-structured membranes prepared from oppositely charged block copolymer nanoparticles and iron oxide nanoparticles. *Journal of Membrane Science* **611**, 118181.

Fukumoto, T., Yoshioka, T., Nagasawa, H., Kanezashi, M. & Tsuru, T. 2014 Development and gas permeation properties of microporous amorphous TiO_2–ZrO_2–organic composite membranes using chelating ligands. *Journal of Membrane Science* **461**, 96–105.

Guo, D., Xiao, Y., Li, T., Zhou, Q., Shen, L., Li, R., Xu, Y. & Lin, H. 2020 Fabrication of high-performance composite nanofiltration membranes for dye wastewater treatment: mussel-inspired layer-by-layer self-assembly. *Journal of Colloid and Interface Science* **560**, 273–283.

Jeon, S. & Lee, J.-H. 2020 Rationally designed in-situ fabrication of thin film nanocomposite membranes with enhanced desalination and anti-biofouling performance. *Journal of Membrane Science* **615**, 118542.

Karami, P., Khorshidi, B., Shamaei, L., Beaulieu, E., o, J., Soares, B. & Sadrzadeh, M. 2020 Nanodiamond-nabled thin-film nanocomposite polyamide membranes for high-temperature water treatment. *ACS Applied Materials & Interfaces* **12** (47), 53274–53285.

Kondoh, M., Moritani, H. & Ishibashi, T. 2020 Observation of translational diffusion in a planer supported lipid bilayer membrane by total internal reflection-transient grating method. *Bulletin of the Chemical Society of Japan* **93** (5), 671–675.

Li, C., Wang, W., Xu, F., Zhang, L. & Yang, W. 2011 Preparation of pH-sensitive membranes via dopamine-initiated atom transfer radical polymerization. *Journal of Membrane Science* **367** (1–2), 7–13.

Luo, J. & Wan, Y. 2013 Effects of pH and salt on nanofiltration – a critical review. *Journal of Membrane Science* **438**, 18–28.

Lv, Y., Yang, H.-C., Liang, H.-Q., Wan, L.-S. & Xu, Z.-K. 2016 Novel nanofiltration membrane with ultrathin zirconia film as selective layer. *Journal of Membrane Science* **500**, 265–271.

Marchetti, P., Jimenez Solomon, M. F., Szekely, G. & Livingston, A. 2014 Molecular separation with organic solvent nanofiltration: a critical review. *Chemical Reviews* **114** (21), 10735–10806.

Mi, Y., Wang, J., Yang, Z., Wang, Z., Wang, H. & Yang, S. 2014 A simple one-step solution deposition process for constructing high-performance amorphous zirconium oxide thin film. *RSC Advances* **4** (12), 6060–6067.

Mi, Y.-F., Xu, G., Guo, Y.-S., Wu, B. & An, Q.-F. 2020 Development of antifouling nanofiltration membrane with zwitterionic functionalized monomer for efficient dye/salt selective separation. *Journal of Membrane Science* **601**, 117795.

Mohammad, A. W., Teow, Y., Ang, W., Chung, Y., Oatley-Radcliffe, D. & Hilal, N. 2015 Nanofiltration membranes review: recent advances and future prospects. *Desalination* **356**, 226–254.

Nazia, S., Sekhar, S. C., Jegatheesan, V., Bhargava, S. K. & Sridhar, S. 2020 Performance of chemically resistant polyurea reverse osmosis membrane in the treatment of highly alkaline industrial wastewater containing sodium aluminate. *Water Science and Technology* **82** (11), 2259–2270.

Nazir, U., Saleem, S., Nawaz, M., Sadiq, M. A. & Alderremy, A. 2020 Study of transport phenomenon in Carreau fluid using Cattaneo–Christov heat flux model with temperature dependent diffusion coefficients. *Physica A: Statistical Mechanics and its Applications* **554**, 123921.

Nigiz, F. & Kibar, M. 2020 UV-assisted desalination of seawater using titanium dioxide nanotube doped polyether block amide membrane. *Water Supply* **20** (6), 2185–2193.

Ou, J., Wang, J., Qiu, Y., Liu, L. & Yang, S. 2011 Mechanical property and corrosion resistance of zirconia/polydopamine nanocomposite multilayer films fabricated via a novel non-electrostatic layer-by-layer assembly technique. *Surface and Interface Analysis* **43** (4), 803–808.

Pavon, S., Fortuny, A., Coll, M., Bertau, M. & Sastre, A. 2020 Permeability dependencies on the carrier concentration and membrane viscosity for Y (III) and Eu (III) transport by using liquid membranes. *Separation and Purification Technology* **239**, 116573.

Polyakov, M. N., Schoeppner, R. L., Pethö, L., Edwards, T. E., Thomas, K., Könnyű, B., Maeder, X. & Michler, J. 2020 Direct co-deposition of mono-sized nanoparticles during sputtering. *Scripta Materialia* **186**, 387–391.

Sanchez, C., Julián, B., Belleville, P. & Popall, M. 2005 Applications of hybrid organic–inorganic nanocomposites. *Journal of Materials Chemistry* **15** (35–36), 3559–3592.

Siddique, H., Rundquist, E., Bhole, Y., Peeva, L. & Livingston, A. 2014 Mixed matrix membranes for organic solvent nanofiltration. *Journal of Membrane Science* **452**, 354–366.

Siddique, T., Dutta, N. K. & Roy Choudhury, N. 2020 Nanofiltration for arsenic removal: challenges, recent developments, and perspectives. *Nanomaterials* **10** (7), 1323.

Singh, M. K. & Mehata, M. 2020 Enhanced photoinduced catalytic activity of transition metal ions incorporated TiO_2 nanoparticles for degradation of organic dye: absorption and photoluminescence spectroscopy. *Optical Materials* **109**, 110309.

Somvanshi, S. B., Kharat, P. B., Khedkar, M. V. & Jadhav, K. 2020 Hydrophobic to hydrophilic surface transformation of nano-scale zinc ferrite via oleic acid coating: magnetic hyperthermia study towards biomedical applications. *Ceramics International* **46** (6), 7642–7653.

Song, Z., Fathizadeh, M., Huang, Y., Chu, K. H., Yoon, Y., Wang, L., Xu, W. L. & Yu, M. 2016 TiO_2 nanofiltration membranes prepared by molecular layer deposition for water purification. *Journal of Membrane Science* **510**, 72–78.

Spiegler, K. & Kedem, O. 1966 Thermodynamics of hyperfiltration (reverse osmosis): criteria for efficient membranes. *Desalination* **1** (4), 311–326.

Spijksma, G. I., Huiskes, C., Benes, N. E., Kruidhof, H., Blank, D. H., Kessler, V. G. & Bouwmeester, H. J. 2006 Microporous zirconia–titania composite membranes derived from diethanolamine-modified precursors. *Advanced Materials* **18** (16), 2165–2168.

Tofighy, M. A. & Mohammadi, T. 2020 Divalent heavy metal ions removal from contaminated water using positively charged membrane prepared from a new carbon nanomaterial and HPEI. *Chemical Engineering Journal* **388**, 124192.

Van der Bruggen, B., Mänttäri, M. & Nyström, M. 2008 Drawbacks of applying nanofiltration and how to avoid them: a review. *Separation and Purification Technology* **63** (2), 251–263.

Vatanpour, V., Madaeni, S. S., Moradian, R., Zinadini, S. & Astinchap, B. 2012 Novel antibifouling nanofiltration polyethersulfone membrane fabricated from embedding TiO_2 coated multiwalled carbon nanotubes. *Separation and Purification Technology* **90**, 69–82.

Vatanpour, V., Esmaeili, M. & Farahani, M. H. D. A. 2014 Fouling reduction and retention increment of polyethersulfone nanofiltration membranes embedded by amine-functionalized multi-walled carbon nanotubes. *Journal of Membrane Science* **466**, 70–81.

Vinh-Thang, H. & Kaliaguine, S. 2013 Predictive models for mixed-matrix membrane performance: a review. *Chemical Reviews* **113** (7), 4980–5028.

Wang, X.-L., Fang, Y., Tu, C.-H. & Van der Bruggen, B. 2012 Modelling of the separation performance and electrokinetic properties of nanofiltration membranes. *International Reviews in Physical Chemistry* **31** (1), 111–130.

Worou, C. N., Kang, J., Shen, J., Degan, A., Yan, P., Wang, W., Gong, Y. & Chen, Z. 2021a Euler's numerical method for ions rejection reassessment of a defect-free synthesized nanofiltration membrane with ultrathin titania film as the selective layer. *Coatings* **11** (2), 184.

Worou, C. N., Kang, J., Shen, J., Yan, P., Wang, W., Gong, Y. & Chen, Z. 2021b Runge–Kutta numerical method followed by Richardson's extrapolation for efficient ion rejection reassessment of a novel defect-free synthesized nanofiltration membrane. *Membranes* **11** (2), 130.

Xia, S., Dong, B., Zhang, Q., Xu, B., Gao, N. & Causseranda, C. 2007 Study of arsenic removal by nanofiltration and its application in China. *Desalination* **204** (1–3), 374–379.

Yang, C., Xu, W., Nan, Y., Wang, Y. & Chen, X. 2020a Novel negatively charged nanofiltration membrane based on 4,4′-diaminodiphenylmethane for dye removal. *Separation and Purification Technology* **248**, 117089.

Yang, W.-J., Shao, D.-D., Zhou, Z., Xia, Q.-C., Chen, J., Cao, X.-L., Zheng, T. & Sun, S.-P. 2020b Carbon quantum dots (CQDs) nanofiltration membranes towards efficient biogas slurry valorization. *Chemical Engineering Journal* **385**, 123993.

Yuan, S., Zhang, G., Zhu, J., Mamrol, N., Liu, S., Mai, Z., Van Puyvelde, P. & Van der Bruggen, B. 2020 Hydrogel assisted interfacial polymerization for advanced nanofiltration membranes. *Journal of Materials Chemistry A.* **8** (6), 3238–3245.

Zhang, H., Mao, H., Wang, J., Ding, R., Du, Z., Liu, J. & Cao, S. 2014a Mineralization-inspired preparation of composite membranes with polyethyleneimine–nanoparticle hybrid active layer for solvent resistant nanofiltration. *Journal of Membrane Science* **470**, 70–79.

Zhang, R., Ji, S., Wang, N., Wang, L., Zhang, G. & Li, J. R. 2014b Coordination-driven in situ self-assembly strategy for the preparation of metal–organic framework hybrid membranes. *Angewandte Chemie International Edition* **53** (37), 9775–9779.

Zhang, R., Su, Y., Zhao, X., Li, Y., Zhao, J. & Jiang, Z. 2014c A novel positively charged composite nanofiltration membrane prepared by bio-inspired adhesion of polydopamine and surface grafting of poly(ethylene imine). *Journal of Membrane Science* **470**, 9–17.

Zhao, D. L., Japip, S., Zhang, Y., Weber, M., Maletzko, C. & Chung, T.-S. 2020a Emerging thin-film nanocomposite (TFN) membranes for reverse osmosis: a review. *Water Research* **173**, 115557.

Zhao, D. L., Yeung, W. S., Zhao, Q. & Chung, T.-S. 2020b Thin-film nanocomposite membranes incorporated with UiO-66-NH_2 nanoparticles for brackish water and seawater desalination. *Journal of Membrane Science* **604**, 118039.

Zhao, Z., Liu, B., Ilyas, A., Vanierschot, M., Muylaert, K. & Vankelecom, I. 2021 Harvesting microalgae using vibrating, negatively charged, patterned polysulfone membranes. *Journal of Membrane Science* **618**, 118617.

Zheng, Y.-M., Zou, S.-W., Nanayakkara, K. N., Matsuura, T. & Chen, J. 2011 Adsorptive removal of arsenic from aqueous solution by a PVDF/zirconia blend flat sheet membrane. *Journal of Membrane Science* **374** (1–2), 1–11.

Zinadini, S., Zinatizadeh, A., Rahimi, M. & Vatanpour, V. 2017 Magnetic field-augmented coagulation bath during phase inversion for preparation of $ZnFe_2O_4/SiO_2$/PES nanofiltration membrane: a novel method for flux enhancement and fouling resistance. *Journal of Industrial and Engineering Chemistry* **46**, 9–18.

First received 13 November 2020; accepted in revised form 31 January 2021. Available online 4 March 2021